

STUDIES OF DEFECT STRUCTURE EFFECTS ON THE TRANSPORT PROPERTIES OF PURE CRYSTALLINE *n*-CdS VIA THE TEMPERATURE DEPENDENCE OF PHOTOACOUSTIC AND PHOTOCURRENT SPECTRA

TAMAS DIOSZEGHY† and ANDREAS MANDELIS

Photoacoustic and Photothermal Sciences Laboratory, Department of Mechanical Engineering,
University of Toronto, Toronto M5S 1A4, Canada

(Received 21 April 1986; accepted 29 May 1986)

Abstract—Microphone gas-coupled photoacoustic spectroscopy (PAS) and photocurrent spectroscopy (PCS) have been applied simultaneously to pure high resistivity single crystals of *n*-CdS at room and low temperatures. The PA and PC spectra obtained at open-circuit and with an applied AC or DC transverse electric field were consistent with an enhancement of the non-radiative recombination quantum efficiency at subbandgap wavelengths at room temperature, accompanied by increasing domination of the open circuit PA spectrum by this parameter at lower temperatures. Further evidence of the importance of non-radiative carrier recombinations at intrabandgap defect centers in the generation of the PA and PC signals was obtained upon introducing deliberate mechanical damage to a single crystal of CdS. The PA technique was found to have an advantage over PC spectroscopy in its ability to spectrally resolve completely the observed peaks attributed to the intrinsic band-to-band transition and to the wavelength dependence of the non-radiative quantum yield.

Keywords: Photoacoustic spectroscopy (PAS), photocurrent spectroscopy (PCS), pure cadmium sulfide, non-radiative quantum efficiency, electronic defects, carrier transport, AC electric fields, DC electric fields.

1. INTRODUCTION

The continuous need for nearly perfect II–VI compound semiconducting material lattices for use in microelectronic and optoelectronic device technologies has brought to attention specific problems associated with the tendency of these compounds to form various intrinsic defects and to deviate from stoichiometry, depending on the preparation method [1]. Pure and specially doped CdS single crystals or thin films have found increasing applications as photoconductive, photovoltaic and optoelectronic devices due to the relatively large bandgap of this material. [1–4]. Recent applications with pure CdS as the active element in solid state excitonic lasers at low temperatures [5, 6] have accentuated the demand for defect and impurity-free semiconductors for high optical gain performance. CdS exhibits a complex native defect structure [7] at wavelengths near the bandgap edge at *ca* 2.4–2.5 eV [8, 9]. Wasa *et al.* [10] have shown that significant elucidation of the nature of defect states can be obtained by use of room temperature photoacoustic spectroscopy (PAS) with piezoelectric detection of the signal from the back of CdS samples irradiated with monochromatic light at the front surface. The PA investigation of such states by those authors led to their classification as lumi-

nescent (radiative) and non-luminescent (non-radiative) recombination centers. Hata *et al.* [11, 12] later pointed out that there is a great difference between room temperature PA CdS spectra obtained with a conventional microphone gas-coupled spectrometer and those obtained piezoelectrically with the transducer attached to the back side of the frontally irradiated sample: the former type of spectra was claimed to yield information similar to the fundamental absorption spectrum of CdS, while the latter type exhibited non-radiative peak structure similar to spectra obtained previously by Wasa *et al.* [10]. Very recently Mandelis and Siu [13, 14] performed experimental and theoretical studies of the room temperature microphone gas-coupled PA and PC spectra of photoexcited pure *n*-CdS single crystals, at open-circuit and in the presence of applied transverse AC and DC electric fields. These workers showed that the *n*-CdS PA spectrum is *not equivalent* to the optical absorption spectrum or the PC spectrum of this semiconductor. The PA spectrum exhibited two major features (maxima) in the bandgap and sub-bandgap regions of CdS, which were consistent with interband electronic transitions and the wavelength dependence of the non-radiative quantum efficiency, $\eta_{non-rad}$, due to subbandgap native defect populations in this material.

It was further demonstrated from comparisons between PAS and PCS that PA spectra interpretation is

† On leave from the Department of Physics, Institute of Isotopes, Budapest H-1525, Hungary.

more easily achieved than the PC counterparts, due to the ability of PAS to resolve the intrinsic transition peak by changing the exciting light modulation frequency, which controls its spectral position [13]. A unified theoretical approach [14] yielded good agreement with both PA and PC spectral profiles, thus enhancing the level of confidence regarding the mechanisms invoked for data interpretation.

The present work was motivated by the necessity to acquire an improved physical understanding and controllability of energy dissipation mechanisms due to the subbandgap native defect structure of well characterized pure CdS crystals at low temperatures and defect influence on the transport properties of this material. At these temperatures optoelectronic devices fabricated from this semiconductor operate with higher energy conversion efficiencies and the question of the degree of microscopic, electronic level integrity of the active material is, therefore, crucial.

2. MATERIALS AND INSTRUMENTATION

Samples used in this work were high purity CdS single crystals from Eagle-Pitcher Inc. Miami, Oklahoma, $10 \times 5 \times 1.5 \text{ mm}^3$ in size with nominal resistivity $\rho = 1.3\text{--}1.9 \times 10^5 \text{ Ohm-cm}$. The nominal mobilities were $190\text{--}215 \text{ cm}^2 \text{ V}^{-1} \text{ s}^{-1}$. The crystal growth details were described elsewhere [13]. The grown crystals were annealed in a sulphur atmosphere, which resulted in the high resistivity and a non-stoichiometric excess of S^{2-} ions in the crystalline matrix [7]. The crystals were cut with the optic c -axis parallel to the surface plane. They were etched in 95% by volume of 3M HCl and 5% by volume of 30% H_2O_2 in H_2O to remove any surface damage which might distort the PA spectrum at and below the bandgap energy [15]. Electrical connections were made using an In-Ga mixture at opposite

$5 \times 1.5 \text{ mm}^2$ crystal surfaces. This metal-semiconductor interface was shown to exhibit ohmic characteristics [13].

The cryogenic PA cell was made from a large block of stainless steel as a modified version of the cell described by Boucher and Leblanc [16]. The stainless steel sample holder was fitted with electrical leads and a thermocouple lead. These contacts were made directly onto the sample by using the In-Ga mixture interfaces diffused into the crystal after baking at *ca* 350°C under nitrogen flow for 2 h. A glass plate was inserted between the sample and the backing to prevent electrical shunting. The PA sample cell was housed in a thermally insulating container made with 1" thick walls of urethane foam (Smithcraft Fiberglass Inc. Toronto, Canada) with a steel exterior and cardboard inner surface. The microphone and detection electronics consisted of a modified EG and G Model 6003 photoacoustic cell at room temperature, separated from the cryogenic chamber with a thick 3" long teflon rod having a 1 mm bore drilled at the center for acoustic coupling to the PA sample cell. The optical circuit is shown in Fig. 1. The monochromatized, quasi-randomly polarized light from a 1000 W Xe lamp (Oriel Model 6141) was used to photoexcite a CdS crystal without (or with) inserted polarizers; in the latter case spectra could be obtained with the radiation electric field vector $E \parallel C$ or $E \perp C$. The photocurrent was detected through the voltage drop across a 20 Ohm resistor in series with the high resistivity CdS crystal. All PA and PC spectra were normalized with Xerox toner spectra taken at the appropriate temperature and/or polarization.

3. EXPERIMENTAL AND RESULTS

Three kinds of experiments were performed at room and low temperatures: (a) open-circuit PAS; (b)

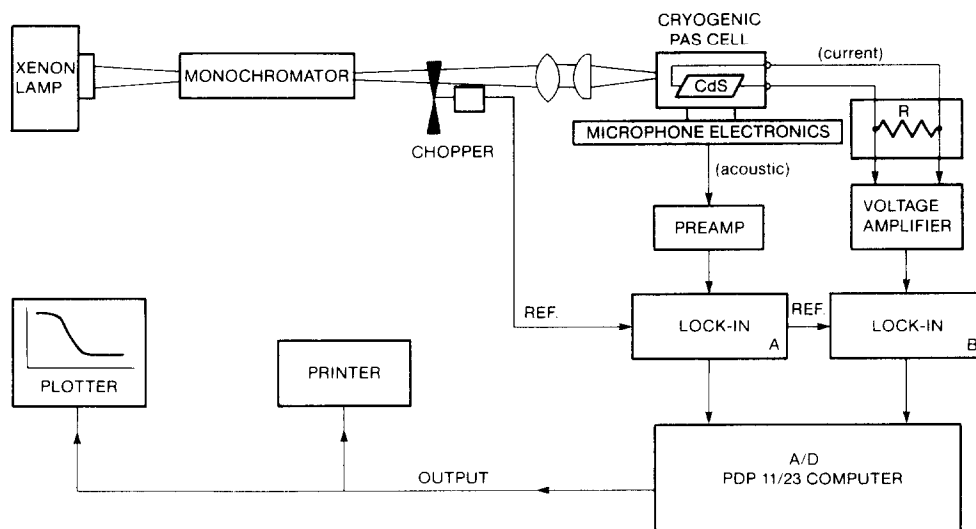


Fig. 1. Schematic diagram of the experimental apparatus for variable temperature PA and PC measurements.

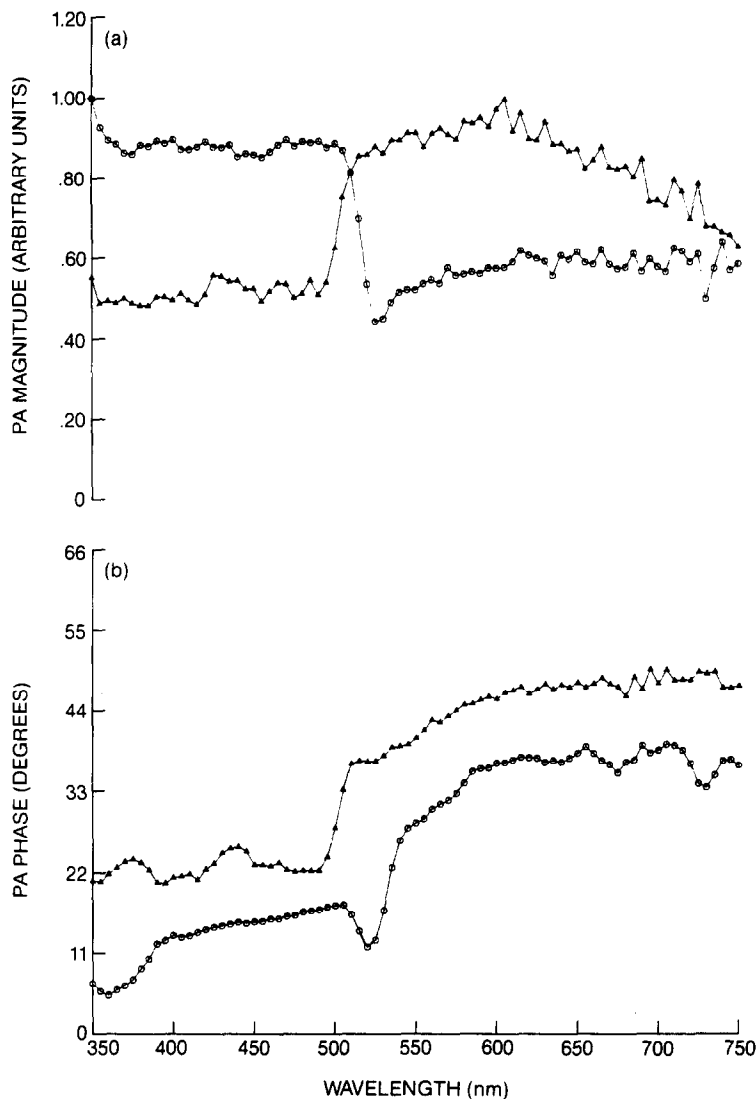


Fig. 2. Open-circuit PA spectra of pure *n*-CdS single crystal: (—○—), $T = 18^{\circ}\text{C}$; (—△—), $T = -160^{\circ}\text{C}$. Light chopping frequency: 30 Hz. Spectral resolution: 8 nm, randomly polarized: (a) magnitude; (b) phase.

PAS and PCS with an applied transverse DC or (c) AC bias. The temperature of the sample could be lowered by pouring liquid nitrogen (LN_2) into the thermally insulating container. Once the desired temperature was reached, the large thermal inertia of the block allowed an essentially isothermal operation of the cell at that temperature for a period long enough to obtain full spectra of CdS in the photon energy region of interest (350–750 nm). Considerable enhancement of the PA signal-to-noise ratio (SNR) was observed if the LN_2 was allowed to evaporate from the insulating container, which eliminated microphonic noise due to boiling. An additional SNR enhancement was obtained at low temperatures upon mildly heating the metal plate supporting the upper PA sample cell window [16] in position. This heating helped decrease light scattering on the window surface by preventing condensation of the ambient water vapor.

3.1. PA absorption spectra at open-circuit

Figure 2 shows open-circuit PA absorption spectra of *n*-CdS at room and low temperatures with random polarization. The $T = 18^{\circ}\text{C}$ PA magnitude and phase exhibit minima at *ca* 525 nm. The $T = -160^{\circ}\text{C}$ phase shows a local minimum at *ca* 520 nm, with no apparent corresponding feature of the low temperature magnitude. The room temperature magnitude behavior at $\lambda \leq 500$ nm and the signal increase at $\lambda \geq 525$ nm are in qualitative agreement with previous observations [13, 17]. Qualitatively similar phase behavior has also been reported by Mandelis and Siu [13] and Takaue *et al.* [18]. The “knee” of the $T = 18^{\circ}\text{C}$ PA magnitude absorption curve at 500 nm in Fig. 2(a) indicates a bandgap value of 2.48 eV. Photoacoustic saturation considerations, however, must be taken into account [13] together with available information on exciton

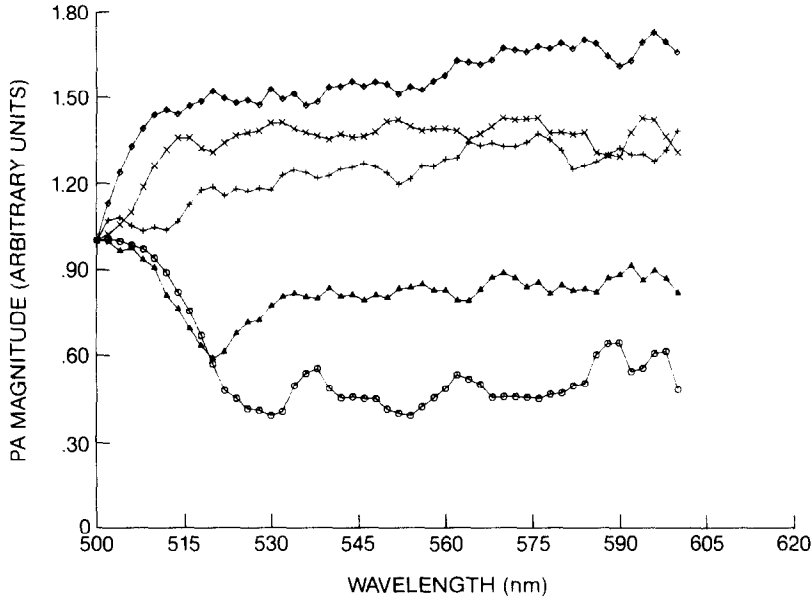


Fig. 3. Open-circuit PA magnitude of pure n -CdS single crystal with temperature as a parameter: (—○—), $T = 22^\circ\text{C}$; (—△—), $T = -23^\circ\text{C}$; (—+—), $T = -73^\circ\text{C}$; (—×—), $T = -116^\circ\text{C}$; (—◇—), $T = -160^\circ\text{C}$. Light chopping frequency: 23 Hz. Spectral resolution: 4 nm, randomly polarized.

formation energies [7], which tend to establish a higher value for the room temperature bandgap energy $E_g \approx 2.56$ eV, in agreement with recent measurements by Davis *et al.* [9] The low temperature PA spectra exhibit a strong inversion due to an increased contribution in the subbandgap region. The high energy “knee” has shifted to 500 nm. Although there is no comparable optical absorption spectrum at -160°C available in the literature, transmission spectra recorded [19] at -183°C (90 K) show the onset of sharp absorption at *ca* 493 nm, with *no inversion*. The PA spectrum of our crystal was further monitored at intermediate temperatures. The PA magnitude results are shown in Fig. 3 with all the curves normalized to the 500 nm value of the room temperature ($T = 22^\circ\text{C}$) spectrum for direct comparison. The data shown in Fig. 3 are the result of smoothing out the experimental data using a smoothing technique [20] in order to reduce the effect of random errors and improve the SNR, especially at the lowest temperatures, $T \leq -73^\circ\text{C}$. According to this technique, each of the data points F_i was replaced by $(F_{i-1} + F_i + F_{i+1})/3$. Table 1 shows the spectral positions of the minima as a function of temperature. The spectral shift of the minima to

higher photon energies is higher than linear, especially at $T < -80^\circ\text{C}$. A meaningful empirical relationship $\lambda_{min} = \lambda_{min}(T)$ cannot be established, however, due to the presence of considerable noise in our system at low temperatures. The PA phases corresponding to Fig. 3 show similar trends with minima generally blue-shifted by 5 nm with respect to those of Table 1 at a given temperature. This $\Delta\lambda \approx 5$ nm blue shift has been previously observed with (0001) CdS PA spectra at room temperature [13].

3.2. PA and PC spectra: modulated optical excitation with DC electric field

Figure 4 shows PA and PC spectra at room temperature in the presence of a transverse DC electric field in the direction perpendicular to that of the incident light. The PA spectra for Fig. 4 have been recorded with quasi-random polarization, with $E \parallel C$ and with $E \perp C$. Quasi-random polarization is the result of the Xe lamp throughput, which exhibits inhomogeneous spectral distributions along the directions parallel and perpendicular to the filament cathode-anode axis. Xerox toner spectra indicated that the overall throughput was approximately twice as large in the perpendicular direction (corresponding to the $E \parallel C$ state) as in the parallel direction (corresponding to the $E \perp C$ state). Moreover, the photon distribution in the perpendicular direction was higher at short wavelengths, while that in the parallel direction was higher at long wavelengths with a cross-over at *ca* 500 nm. The lamp spectrum without polarizers was the weighted average of the two contributing polarizations, not entirely random due to the variable relative spectral weight of each polarization at different wavelengths. Fig. 4(a) shows

Table 1. PA magnitude absorption minima dependence on temperature

| Minimum spectral position (nm) \rightarrow (eV) | Temperature ($^\circ\text{C}$) | |
|---|----------------------------------|------|
| 526 | 2.36 | 22 |
| 520 | 2.38 | -23 |
| 514 | 2.41 | -73 |
| 504 | 2.46 | -116 |
| 490 | 2.53 | -160 |

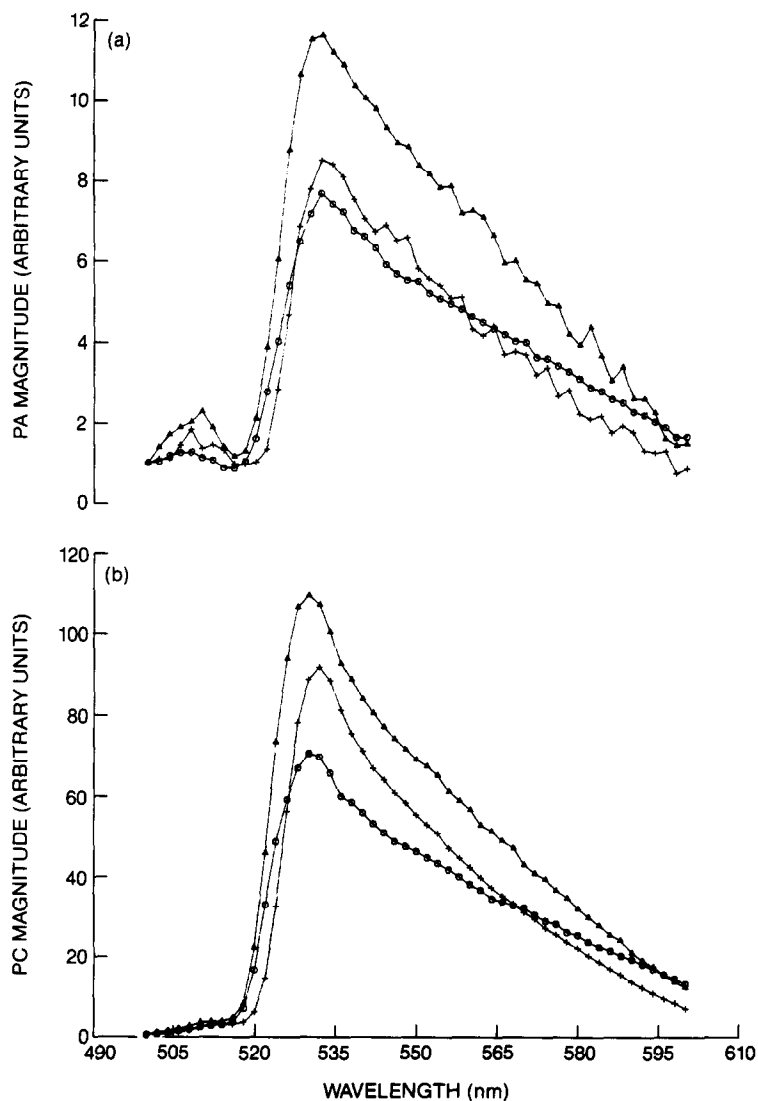


Fig. 4. Magnitudes of (a) PA and (b) PC spectral responses with a transverse electric field of 20 VDC: (—○—), quasi-random polarization; (—+—), $E \perp C$; (—△—), $E \parallel C$. Light chopping frequency: 23 Hz; spectral resolution: 2 nm; $T = 22^\circ\text{C}$.

the onset of the rising edge of the main PA peak at lower energies for $E \perp C$ than for $E \parallel C$. The wavelength difference is $\Delta\lambda \approx 3$ nm. Similar features can be seen in the PC magnitude for Fig. 4(b), which is in agreement with polarization studies of the photoconductivity of pure ("undoped") CdS single crystals reported by Yoshizawa [21] at 77 K and by Park and Reynolds [22] at 293 K and at 77 K. In both PA and PC spectra of Fig. 4, the main peak is located at *ca* 530–532 nm. The PA spectra, however, in addition exhibit a high energy secondary peak at *ca* 508–510 nm. No such peak is visible in the PC spectra, which only show an unresolved shoulder in the same energy range. Similar features have been observed experimentally [13] in the PA and PC spectra of (0001) CdS with the high energy PA peak at *ca* 517 nm, and have been explained theoretically [14] in terms of carrier transport and non-radiative

quantum efficiency spectral dependence mechanisms. The PA and PC phases show similar trends with those of the magnitudes, with respect to spectral shifting with polarization. The quasi-randomly polarized phases are shown in Fig. 5. This Fig. corresponds to the respective curves of Fig. 4 and the PC phase lag is characterized by minima at *ca* 508 nm and 528 nm, as well as a maximum at 518 nm. The PA phase lag, however, increases essentially monotonically at long wavelengths.

The temperature dependence of the PA signal is shown in Fig. 6. The smoothed low temperature spectrum (B) in Fig. 6(a) is blue-shifted by *ca* 26 nm with respect to the room temperature spectrum (A). The acoustic noise associated with the low temperature spectrum did not allow a complete characterization of the secondary high energy peak at that temperature. The position of the main PA peak is at

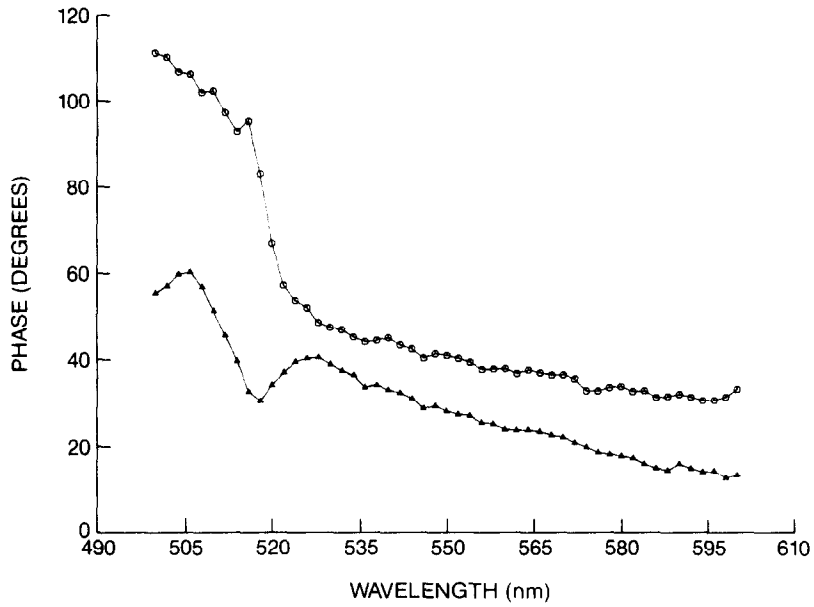


Fig. 5. Quasi-randomly polarized PA, (—○—) and PC, (—△—) phases corresponding to Fig. 4.

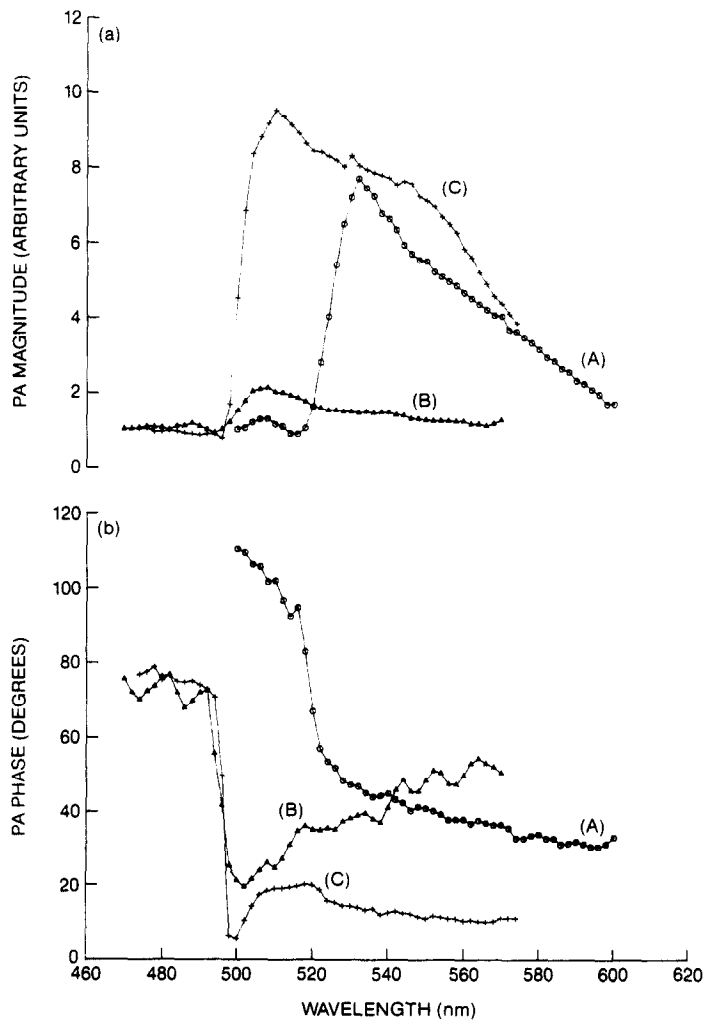


Fig. 6. Magnitudes (a) and phases (b) of PA with a transverse electric field of 20 VDC; curves (A): $T = 22^\circ\text{C}$; curves (B): $T = -160^\circ\text{C}$ smoothed spectra; curves (c): $T = -160^\circ\text{C}$, after fracture. Light chopping frequency: 23 Hz; spectral resolution: 2 nm. All magnitude spectra normalized to the same value at 470 nm.

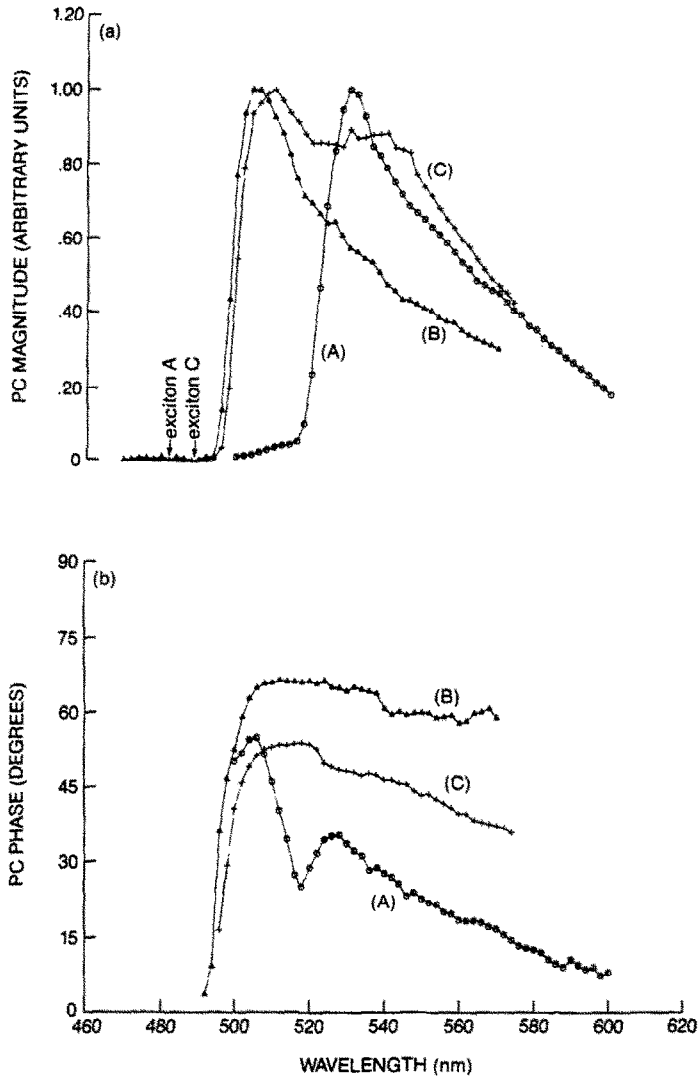


Fig. 7. Magnitudes (a) and phases (b) of PC spectra with a transverse electric field of 20 VDC; curves (A): $T = 22^\circ\text{C}$; curves (B): $T = -160^\circ\text{C}$; curves (C): $T = -160^\circ\text{C}$, after fracture. Light chopping frequency: 23 Hz; spectral resolution: 2 nm. All magnitude spectra normalized to the same peak value.

506 nm. Spectrum (C) was taken after deliberate mechanical damage was introduced in the crystal through fracture. The PA signal enhancement was substantial, so no need for smoothing the spectrum arose. In comparison with spectrum (B) the greatest enhancement was observed in the subbandgap region, $\lambda \geq 510$ nm. This PA magnitude increase was accompanied by a phase lag increase at $\lambda \geq 520$ nm, as shown in Fig. 6(b), curve (C). Figure 7 shows the temperature dependence of the simultaneously obtained PC signal. No smoothing out at low temperatures was necessary with PC spectra, as they were not affected by acoustic noise. The $T = -160^\circ\text{C}$ spectrum of the intact crystal shows a very low signal at photon energies above 2.51 eV with two minima at ca 482 nm and 488 nm. Our tentative assignments of these minima are those of exciton A and C absorption lines, respectively; Gross and Novikov [23] established a correlation between the exciton

emission spectrum and the PC spectrum. These authors showed that all pure CdS crystals can be divided into two groups: in crystals of the first group exciton absorption lines at 487 and 479 nm at 77 K were associated with PC maxima, and in crystals of the second group these same wavelengths were associated with PC minima. At 77 K Uchida [7] placed excitons A, B and C at 487.5, 484.5 and 472.5 nm, respectively. At -160°C and using the temperature coefficient of all three exciton photo-conductivities established by Uchida ($= 3 \times 10^{-4} \text{ eV/K}$), PC minima due to A and C exciton absorption and thermal release to the conduction band are expected at 489 nm and 482 nm, respectively, for crystals of the second group, consistently with the PC spectrum of Fig. 7, curve (B). No PC minima could be observed in the low temperature spectrum of the fractured crystal in Fig. 7, curve (C). Subbandgap wavelength sensitization, however, of

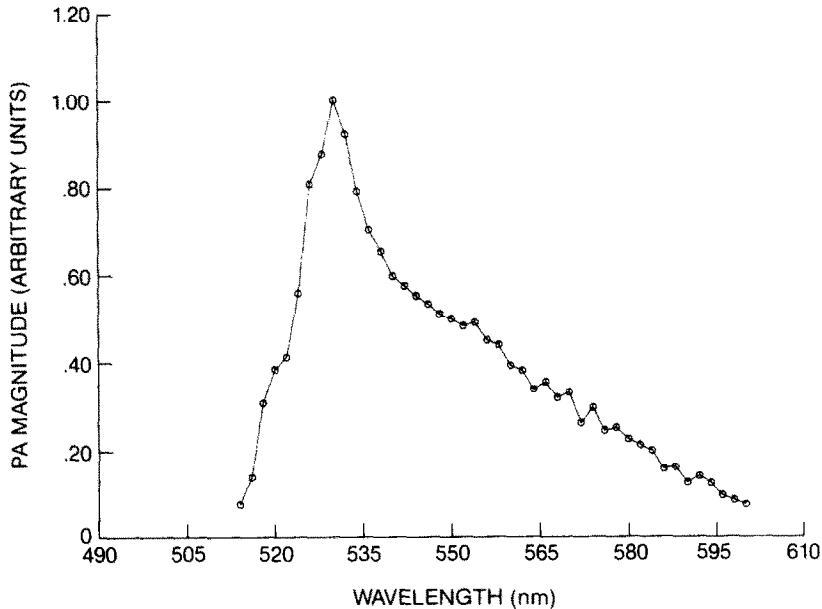


Fig. 8. PA magnitude with a transverse AC electric field of 20 V peak-to-peak and quasi-randomly polarized unmodulated light. Electric field modulation frequency: 23 Hz; spectral resolution: 4 nm; $T = 20^{\circ}\text{C}$.

the PC spectrum of the damaged crystal was observed with spectral features similar to those of the PA spectrum in Fig. 6, curve (C).

3.3. PA and PC spectra: unmodulated optical excitation with an AC electric field

This type of measurement was performed on the pure CdS crystal before and after mechanical damage. Figure 8 shows the PA magnitude corresponding to the intact crystal at 20°C . At low temperatures the PA signal of this crystal was too low to be conclusively recorded. In Fig. 8 a new shoulder has appeared at $\lambda \leq 522$ nm, which merges with the main peak at 530 nm. The secondary peak observed at ca 508 nm in Fig. 6(a) is not present under this mode of optical excitation. Similar phenomena have been reported previously [13] for (0001)-oriented pure *n*-CdS crystals. The PC magnitude showed evidence of a shoulder at $\lambda \leq 522$ nm. High resolution ($\Delta\lambda = 2$ nm), good quality PA spectra were obtained with the lock-in analyzer tuned to twice the electric field modulation frequency, due to the Joule effect, which was found to dominate the PA signal [13, 14] at subbandgap wavelengths in this experimental mode. These spectra are *not identical* to those obtained at $1f$, Fig. 8, however, they share common features. Figure 9 shows PA and PC spectra obtained simultaneously at $2f$ at 20°C with the intact crystal. The secondary PA peak at ca 515 nm appears merging with the main peak at ca 532 nm in close correspondence to the $1f$ spectrum of Fig. 8. The main difference between the $1f$ and $2f$ room temperature PA spectrum is the increased FWHM of the main absorption band of the $2f$ spectrum, Fig. 9(a), compared to that of Fig. 8. Figure 10 shows the $2f$ PC

signum magnitude at -160°C . No $2f$ PA spectrum could be obtained due to the smallness of the signal amplitude at this temperature. The PC spectral maximum is shifted by ca 34 nm to 498 nm compared to Fig. 9(a) and the FWHM exhibits a substantial decrease from 57 nm down to 15 nm.

After fracture of the CdS crystal, the low temperature PA signals increased dramatically as shown in Fig. 11, in which the $1f$ PA and PC spectra are plotted at -163°C . The PA spectrum at $\lambda > 500$ nm exhibits a relative enhancement compared to the PC spectrum. A similar observation is valid for $\lambda < 488$ nm. The $2f$ spectra generally exhibit similar features to the $1f$ spectra as shown in Fig. 12.

4. DISCUSSION

The PA absorption spectra, Fig. 2, have been found to be different from optical transmission spectra in that they do not strictly anticorrelate with the latter spectra at subbandgap wavelengths ($\lambda > 525$ nm at $T = 18^{\circ}\text{C}$). The room temperature PA signal past the minimum, at $\lambda \geq 525$ nm, has been attributed [13] to a substantial increase in the non-radiative quantum efficiency associated with the carrier recombination process. This mechanism, when incorporated in a theoretical model coupling the PA and PC spectral responses [14], gave satisfactory agreements with the experimental data. A similar enhancement of the non-radiative quantum yield in Ge doped As_2Se_3 glasses, materials with rich defect state structure at energies below the optical gap, has been measured photoacoustically by Kitamura *et al.* [24]. Pure *n*-CdS is also defect rich in the subbandgap region, owing to the preparation process which cre-

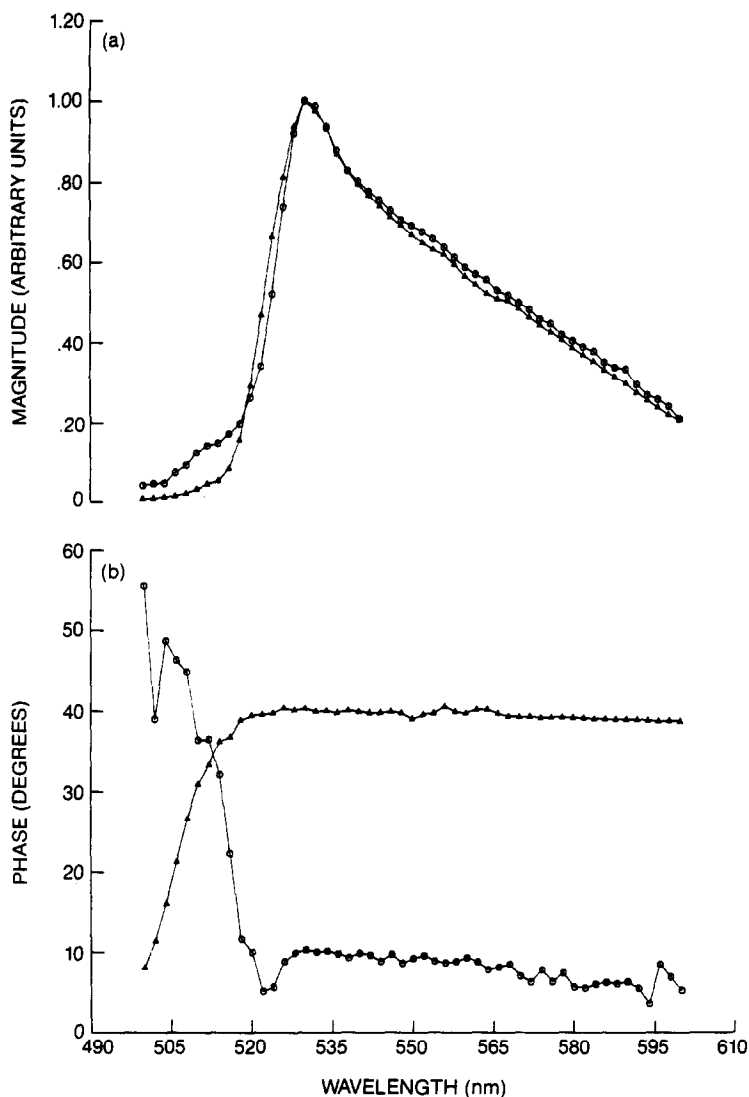


Fig. 9. Magnitudes (a) and phases (b) of PA and PC spectra at $2f$ with a transverse AC electric field of 20 V peak-to-peak and quasi-randomly polarized unmodulated light. Electric field modulation frequency $f = 23$ Hz; spectral resolution: 2 nm; $T = 20^\circ\text{C}$. (\circ), PA spectrum; (\triangle), PC spectrum. Magnitudes matched arbitrarily at 532 nm.

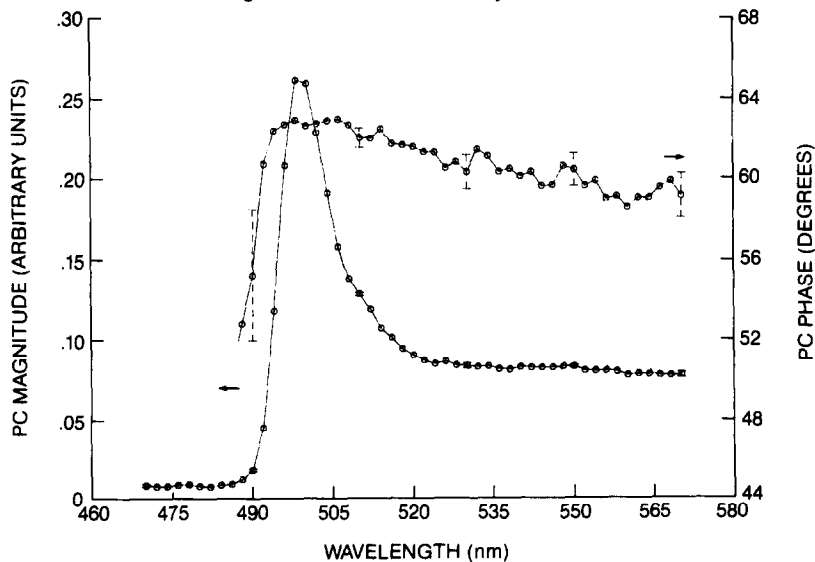


Fig. 10. PC signal magnitude and phase recorded at $2f$ with intact pure n -CdS in the presence of a transverse AC electric field of 20 V peak-to-peak; $T = -160^\circ\text{C}$.

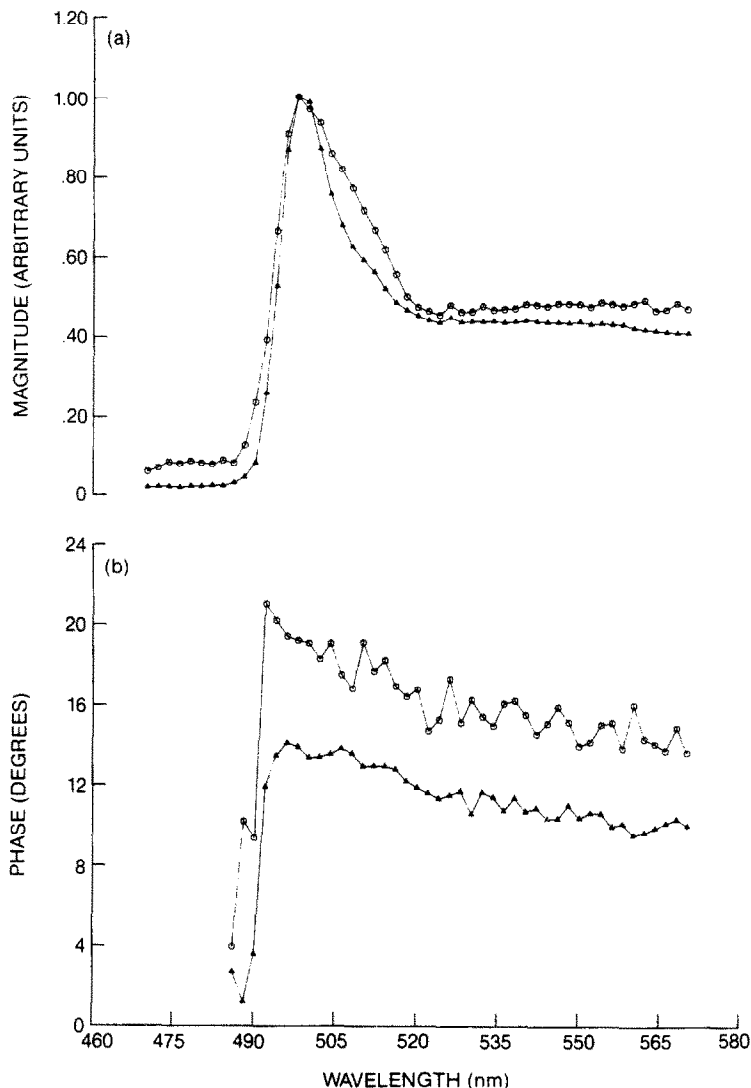


Fig. 11. Magnitudes (a) and phases (b) of PA and PC spectra at $1f$ with a transverse AC electric field of 20 V peak-to-peak and quasi-randomly polarized unmodulated light. Electric field modulation frequency $f = 23$ Hz; spectral resolution: 2 nm; $T = -163^\circ\text{C}$. (\circ — \circ), PA spectrum; (\triangle — \triangle), PC spectrum. Magnitudes matched arbitrarily at 498 nm.

ates large densities of native defects, such as sulphur vacancies when the crystal is annealed in a sulphur atmosphere [7]. The defect mediated recombination processes contribute a small fraction of the PA signal at room temperature, compared to the intrinsic excitation contributions at photon energies at, or above, the bandgap value; these processes, however, tend to dominate the PA magnitude response at cryogenic temperatures as shown in Fig. 2(a). The gradual nature of the spectral inversion, Fig. 3, with decreasing temperature would tend to support a monotonic increase in subbandgap photosensitivity at lower temperatures, in agreement with experimental observations of the low temperature sensitization of the photoconductivity by Bube and Barton [25]. These authors showed that the degree of subbandgap sensitization at low temperatures was

a sensitive function of the defect history of CdS samples and that it increased dramatically with the inclusion of trace impurities, such as iodine. Bube [26] further showed from the analysis of the photocurrent temperature dependence, that a rapid decrease in CdS photosensitivity occurs at temperatures where the location of the Fermi level falls below 0.6 eV under the conduction bandedge. Our open circuit spectra show that PAS can be used as a very sensitive tool to monitor the degree of sensitization at low temperatures where the defect structure of CdS dominates the visible PA spectrum. The PA phase lag of Fig. 2(b) shows features similar to those reported previously [13, 18]. The minimum at *ca* 525 nm of the $T = 18^\circ\text{C}$ curve is probably the result of the interplay between (i) the motion of the heat centroid, which is receding from the crystal surface into the bulk at long

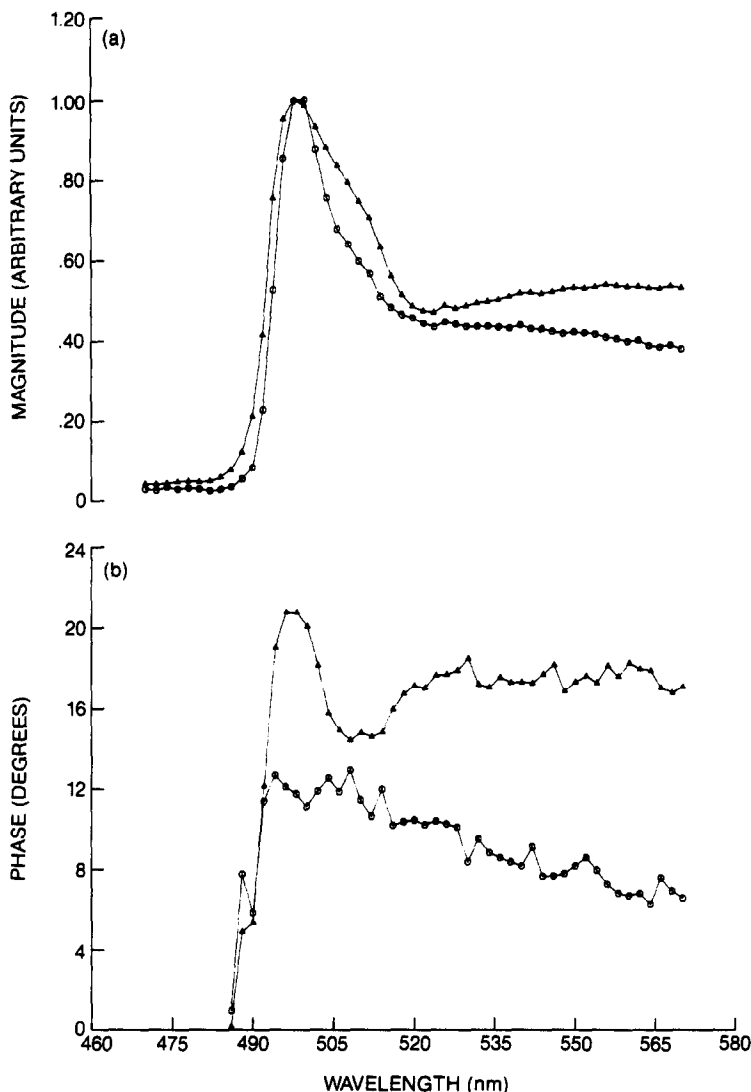


Fig. 12. Same as Fig. 11 with spectra recorded at $2f$.

wavelengths with decreasing optical absorption coefficient, and (ii) the rapid increase of the recombination non-radiative quantum efficiency, which is essentially a surface phenomenon with significant contributions from the surface state density of the material. The phase lead at $\lambda \geq 550$ nm compared to phase values at $\lambda \leq 500$ nm is a further indication of the bulk nature of PA spectra even in spectral regions of large optical absorption coefficients, since [27] the depth of spectral information at $\lambda \leq 500$ nm is governed by the thermal diffusion length (*ca* 0.3 mm at 30 Hz) rather than the photoacoustically saturated optical absorption depth in CdS (*ca* 12.5 μm at 480 nm) [19]. At $T = -160^\circ\text{C}$ the decreased importance of the superbandgap recombination contributions to the PA signal has all but eliminated the phase lag minimum, indicating a steeper increase of the subbandgap quantum efficiency with increasing wavelength. The significance of some of the minor features of the low temperature PA spectra in Figs 2

and 3 may not be assessed from the present results due to the low SNR at those temperatures. When put in perspective, however, the microphone gas-coupled method of detection appears to be preferable to the piezoelectric transducer method at cryogenic temperatures. The latter method has been reported [28] to be inappropriate to use below 195 K for regular PA absorption spectra acquisition, however, a strong signal from the U-peak of undoped InSe has been recently [29] obtained satisfactorily at 100 K.

The PA polarized spectra of Fig. 4 show evidence of the excitonic structure superimposed over the room temperature high energy secondary peak at *ca* 508–512 nm. According to the quantum mechanical selection rule of CdS interband transitions [30], such transitions from the A valence band are forbidden for optical excitation with $E \parallel C$; allowed transitions from the B and C bands could be responsible for the single peak at $\lambda = 512$ nm in the $E \parallel C$ spectrum of Fig. 4(a). All transitions from the A, B and C bands are

allowed for $E \perp C$, which could account for the appearance of two peaks at 510 nm and 514 nm in the $E \perp C$ spectrum. The quasi-randomly polarized spectrum of Fig. 4(a) seems to yield an averaged signal over all the peaks with a maximum at *ca* 508 nm. Wasa *et al.* [10] were also able to resolve the excitonic contributions to the PA signal of CdS as a function of incident light polarization, using piezoelectric backside detection and exploiting the capability of that mode for monitoring non-radiative transition bands. No excitonic evidence is seen in the PC spectra of Fig. 4(b). The PA and PC spectral maxima at *ca* 530–532 nm have been associated [13, 14] with the attainment of the maximum value (saturation) of the recombination process non-radiative quantum efficiency. The large ratio of the main to secondary PA peak intensities in Fig. 4(a) (≈ 6.5) is likely to be indicative of the more prominent role of recombination related defects in our material than in the well-characterized (0001)-oriented *n*-CdS crystals used by Mandelis and Siu [13, 14]. Specifically, parameter variations aimed at simulating the PA and PC spectral features of CdS through a rigorous solution of the carrier transport equations using finite differences [14], indicated that the cause of the large peak ratio in this work can *only* be one or more of the following factors: (i) a large surface recombination velocity; (ii) a high intrabandgap density of carrier traps acting as recombination centers; and/or (iii) a short carrier lifetime. The latter two parameters are generally expected to be wavelength dependent in the spectral range of interest [26, 31]. The spectral position of the main peak at 530–532 nm remains essentially fixed when the chopping frequency of the light intensity is varied. The secondary peak exhibits a blue shift of a few nanometers with increasing frequency as predicted by the theory by Bandeira *et al.* [32] for the PA peak maximum associated with the intrinsic band-to-band transition in CdS. The PA phase lag of Fig. 5 increases monotonically at subbandgap wavelengths due to the domination of the heat generation mechanism by the bulk Joule effect at the applied electric field of 20V DC [13, 32]. The effect of the subbandgap non-radiative quantum efficiency enhancement may not be negligible in our crystal, unlike previous reports [13, 14] with (0001) *n*-CdS, which could explain the slight PA phase dependence on wavelength at $\lambda > 520$ nm. It was further found from the (0001) *n*-CdS PC phase spectrum [13] that the PC phase lag increased monotonically with λ in that spectral range. The presence of a PC phase lag maximum at 518 nm in Fig. 5 supports the contention that the $\eta_{non-rad}$ may not be negligible in comparison with the Joule effect in our experiments and, as a mainly surface-related contribution to the PC signal, tends to decrease the phase lag at $\lambda > 518$ nm. This interplay results in a spectral phase inversion for $518 \text{ nm} \leq \lambda \leq 528 \text{ nm}$, with the Joule effect dominating the PC phase at longer wavelengths. It is interesting to note that the PA

phase spectrum, itself being shaped by mainly bulk-related thermal diffusion effects, is less sensitive to surface-related $\eta_{non-rad}$ contributions in Fig. 5. The main effect of non-negligible $\eta_{non-rad}$ appears to enter in preventing the PA phase from saturating as early as 525 nm as reported previously by Mandelis and Siu [13]. At $T = -160^\circ\text{C}$, however, the increased contributions to the PA signal from subbandgap defect centers, which created the spectral inversion of Fig. 2(a), can still be seen to influence the PA phase spectrum of Fig. 6(b), curve (B), by exhibiting a substantial decrease in the phase lag at $\lambda > 500$ nm. This monotonic phase lag decrease is consistent with an increasing domination of the PA signal by defect site recombinations at long wavelengths, a process heavily weighed by contributions from or near the crystal surface region. This process can be considered to be superimposed on the Joule effect in Fig. 6(b), curve (B). The contribution of the Joule effect to the PA signal generation is expected to be smaller at $T = -160^\circ\text{C}$ than at room temperature due to the increased mean free paths of carriers at this temperature. The interplay between roughly similar thermal contributions from the crystal bulk (Joule effect) and the surface (defect center recombination) would result in a PA phase lag spectral maximum at $T = -160^\circ\text{C}$, such as the one at *ca* $\lambda = 502$ nm in Fig. 6(b), curve (B). The surface-related PC phase at -160°C , Fig. 7(b), curve (B), is seen to be completely dominated by defect center recombinations from or near the surface and thus becomes essentially independent of wavelength at $\lambda \geq 505$ nm.

In the light of the above discussion, the introduction of spatially deep-lying defects through fracture of the CdS crystal can be expected to decrease the bulk carrier mean free path and therefore enhance the Joule effect contribution at cryogenic temperatures. Figures 6 and 7 bear out this expectation. The strength of the overall PA magnitude of the damaged crystal in Fig. 6(a), curve (C), has increased approximately tenfold over that of the intact crystal, with the most notable relative increase in the subbandgap region, $\lambda \geq 505$ nm. The PA phase lag of the damaged crystal in Fig. 6(b), curve (C), does show an initial decrease with increasing λ above the 500 nm maximum similar to that of the intact crystal, however, as the source photon flux decreases at longer wavelengths the bulk Joule effect, enhanced in the damaged crystal, dominates the heat release due to the trap center recombination of the decreasing free carrier densities and the phase lag shows a minimum at *ca* 520 nm. This wavelength is also associated with the onset of significant subbandgap PA and PC magnitude contributions in Figs 6(a) and 7(a), curves (C). The PC magnitude enhancement of the damaged crystal is also very large in the subbandgap region where the crystal is photosensitized, Fig. 7(a), curve (C). The PC phase lag of Fig. 7(b), curve (C) shows an increase with increasing wavelength for $\lambda > 522$ nm, an indication of enhanced bulk Joule

effect contributions to this signal channel at long wavelengths where the effect of crystalline damage is most pronounced.

In the experimental mode using unmodulated optical excitation of CdS in the presence of an applied transverse AC electrical field, *only* the thermal energy release due to the Joule effect contributes to the photoacoustic signal and only those carriers surviving collisional deexcitations contribute to the AC photocurrent signal. This simplified situation occurs because thermal energy from non-radiative carrier recombination is not temporally modulated and therefore will not be subject to PA and PC lock-in detection. This method has been proven to give simple interpretations of experimental CdS spectral responses and to help in elucidating signal generation mechanisms [13, 14]. The existence of strong PA and PC signals at lock-in detection frequencies $1f$ (equal to the electric field modulation frequency) and $2f$ (characteristic of Joule heating, due to the dependence of the bulk crystal heating rate on the square of the alternating electric field [14]) in Figs 8–12 indicates the presence of a strong Joule effect factor throughout the CdS spectral range of interest (500–600 nm). Both the $1f$ and $2f$ channel PA magnitudes at room temperature in Figs 8 and 9(a) exhibit a maximum and an unresolved shoulder. A comparison with the room temperature PA magnitude of Fig. 6(a), curve (A), shows that the long wavelength maxima are located at 530–532 nm, i.e. in essentially the same spectral position, while the peak position of the shoulder in Fig. 8 is located at $\lambda \geq 522$ nm, a shift of *ca* 14 nm or more from the secondary peak at 508 nm in Fig. 6(a), curve (A). The PC magnitudes, however, exhibit similar spectral features under both chopped and unmodulated illumination, Figs 7(a), curve (A), and 9(a), with the trace of the high energy side shoulder evident in the PC spectrum of Fig. 9(a) at $\lambda \approx 510$ nm. Similar trends recently observed [13] with (0001) *n*-CdS were explained by associating the spectral shift of the high photon energy peak [equivalent to the 508 nm peak in Fig. 6(a), curve (A)] to longer wavelengths [e.g. to $\lambda \geq 522$ nm in Fig. 9(a)], with the electric field modulation frequency dependence of the PA signal. The high energy side peak of Fig. 6(a), curve (A), was attributed to the band-to-band electronic transition, and its spectral position in Figs 8 and 9(a) was found to be consistent with the theory by Bandeira *et al.* [32], upon regarding the latter spectra as the limiting case of $f_0 = 0$ Hz; f_0 stands for the light chopping frequency. It is the qualitative agreement of the red shift of the 508 nm peak with the model by Bandeira *et al.* [32] that identifies unambiguously the origin of this peak as due to the intrinsic transition. The independence of the 530 nm peak from the field modulation frequency is consistent with the spectral variation of $\eta_{\text{non-rad}}$, a quantity not dependent on the modulation frequency [14]. Further support to this interpretation is given by the PC magnitude spectral

similarity in Figs 7(a), curve (A), and 9(a). This similarity can be understood from the fact that the PC response is independent of the photoacoustic thermal diffusion length [27], which is ultimately responsible for the red shift of the intrinsic PA shoulder at $f_0 \rightarrow 0$ Hz. The increase in the PA phase lag in Fig. 9(b) can be explained by the Joule effect caused by a receding heat centroid from or near the surface into the bulk with increasing wavelengths [13]. Similarly, the PC phase lag in Fig. 9(b) is essentially surface controlled as seen by the steep decrease at $\lambda > 500$ nm, and becomes independent of wavelength at $\lambda > 520$ nm. This is consistent with this channel's dependence on the carrier diffusion length only [13], a material characteristic parameter independent of the wavelength of the exciting radiation.

Unfortunately, the cryogenic PA signal from the intact crystal was also too low to measure with this mode of experimentation. The PC signal of Fig. 10 recorded at $2f$ shows a remarkable line narrowing compared to the room temperature spectrum. This is the result of diminished contributions of the Joule effect to the photocurrent at long wavelengths due to freezing in of thermal excitations to the conduction band from intrabandgap defect states, such as the doubly ionized donor state V_{2+} identified by Uchida [7]. Figures 11 and 12 show the PA signals from the damaged crystal. With this mode of experimentation, the spectral peak has considerably smaller FWHM than its counterpart in Fig. 6(a), curve (C). This is a consequence of the fact that this mode is only sensitive to Joule heating and carries no information about surface recombination related thermal effects or intrinsic band-to-band recombinations [32]. Therefore, a comparison of the details of the spectral shapes between Figs 11(a) and 6(a), curve (C), can, in principle, deconvolute the Joule effect from other contributions to the PA signal. The monotonic increase of the low temperature PA phase lags with increasing λ at energies below E_g in Figs 11(b) and 12(b), is an indication of the domination of the Joule effect in the region $\lambda > 490$ nm, with small contributions from other damage related defects. No maximum comparable to the one shown in the phase spectrum of Fig. 6(b), curve (C), followed by a minimum, can be seen here within experimental error. This fact indicates the absence of any strong interplay between thermal sources in different spatial locations, as expected. Spectral oscillations of the PC phase about a virtual axis parallel to the wavelength axis in the subbandgap region shown in the $2f$ channel of Fig. 12(b) are difficult to interpret. They are probably related to the substantial enhancement of the $2f$ PC signal at $502 \text{ nm} \leq \lambda \leq 520 \text{ nm}$ relative to the $1f$ magnitude and the resulting broadening of the $2f$ PC band. This phenomenon is likely to carry information on the impact of the crystal defect structure on carrier scattering dynamic mechanisms and is currently under investigation.

5. CONCLUSIONS

This work has shown that microphone gas-coupled PAS can be used at low temperatures as a sensitive detector of the photosensitization of CdS single crystals by the native defect structure of this material. In the presence of DC electric fields, the two resolved PA peaks in the range 505–535 nm at room temperature were found to be interpretable in terms of assignments made by Mandelis and Siu [13, 14]. PCS was unable to resolve these peaks, and thus the use of PAS was found to be advantageous, with the modulation frequency controlling peak separation. Both the Joule effect and wavelength dependence of the recombination process non-radiative quantum efficiency were found to be responsible for shaping the subbandgap PA and PC spectral responses (magnitude and phase lag) upon application of transverse DC electric fields. Joule effect contributions to the low temperature PA signals of a damaged crystal were shown to be enhanced in comparison to PA responses from the intact crystal, especially in the subbandgap region. The application of transverse AC electric fields was found to be capable of deconvoluting the Joule effect contributions to the PA signal from other non-radiative mechanisms and, therefore, of directly studying the scattering mechanisms which set limitations on the magnitude of the PC response and the crystal quantum efficiency. A most important characteristic of the low temperature PAS of CdS crystals has been shown to be the enhanced signal due to defect center carrier recombinations, which renders this technique into a unique and powerful direct method for defect physics studies in this and other crystalline and amorphous semiconductors.

Acknowledgements—The authors wish to acknowledge the financial support of the Natural Sciences and Engineering Research Council of Canada (NSERC) throughout the duration of this work. Tamas Dioszeghy is grateful to the Hungarian Academy of Sciences for a grant which made this research possible. E. Siu's assistance with the defect crystal measurements and R. Wagner's help with computer data reduction are gratefully acknowledged.

REFERENCES

1. Georgobiani A. N., *Soviet Phys.-Usp.* **17**, 424 (1974).
2. Bube R. H., *Photoconductivity of Solids*, p. 391. Wiley, New York (1960).
3. Basov N. G., Bogdankevich O. V. and Devyatkov A. G., *Soviet Phys.-JETP* **20**, 1067 (1965).
4. Reynolds D. C. and Czyzak S. J., *Phys. Rev.* **96**, 1705 (1954).
5. Wünnstel K. and Klingshirn C., *Opt. Commun.* **32** 269 (1980).
6. Song J. J. and Wang W. C., *J. appl. Phys.* **55**, 660 (1984).
7. Uchida I., *J. phys. Soc. Japan* **22**, 770 (1967).
8. Klick C. C., *Phys. Rev.* **89**, 274 (1953).
9. Davis J. J., Cox R. T. and Nicholls J. E., *Proc. 13th Intl. Conf. Defects in Semiconductors* (Edited by L. C. Kimerling and J. M. Parsey Jr.), p. 1237. Metallurgical Soc. AIME Publ. (1985).
10. Wasa K., Tsubouchi K. and Mikoshiba N., *J. appl. Phys. Japan* **19**, L475 (1980).
11. Hata T., Sato Y. and Kurebayashi M., *J. appl. Phys. Japan* **22**, Suppl. 22-3, 205 (1982).
12. Hata T., Sato Y., Nagai Y. and Hada T., *J. appl. Phys. Japan* **23**, Suppl. 23-1, 75 (1983).
13. Mandelis A. and Siu E. K. M., *Phys. Rev. B* (in press).
14. Siu E. K. M. and Mandelis A., *Phys. Rev. B* (in press).
15. Hata T., Hatsuda T., Kawakami M. and Sato Y., *J. appl. Phys. Japan* **24**, Suppl. 24-1, 204 (1985).
16. Boucher F. and Leblanc R. M., *Can. J. Spectrosc.* **26**, 190 (1981).
17. Bard A. J., *Analysis* **6**, 277 (1978).
18. Takaue R., Matsunaga M. and Hosokawa K., *J. appl. Phys.* **56**, 1543 (1984).
19. Dutton D., *Phys. Rev.* **112**, 785 (1958).
20. McCracken D. D. and Dorn W. S., *Numerical methods and FORTRAN programming*. Wiley, New York (1964).
21. Yoshizawa M., *J. appl. Phys. Japan* **15**, 2143 (1976).
22. Park Y. S. and Reynolds D. C., *Phys. Rev.* **132**, 2450 (1963).
23. Gross E. F. and Novikov B. V., *Fiz Tverd. Tela* **1**, 357 (1959).
24. Kitamura M., Ogawa T. and Arai T., *J. phys. Soc. Japan* **52** 2561 (1983).
25. Bube R. H. and Barton L. A., *RCA Rev.* **111**, 564 (1959).
26. Bube R. H., *Phys. Rev.* **99**, 1105 (1955).
27. Rosencwaig A. and Gersho A., *J. appl. Phys.* **47**, 64 (1976).
28. Ikari T., Shigetomi S., Koga Y. and Shigetomi S., *J. Phys. C: Solid St. Phys.* **17**, L969 (1984).
29. Shigetomi S., Ikari T., Koga Y. and Shigetomi S., *Phys. Status Solidi A* **90**, K61 (1985).
30. Hopfield J. J., *J. Phys. Chem. Solids* **15**, 97 (1960).
31. Lambe J., *Phys. Rev.* **98**, 985 (1955).
32. Bandeira I. N., Closs H. and Ghizoni C. C., *J. Photoacoust.* **1**, 275 (1982).